Journal of Materials Chemistry A

Accepted Manuscript

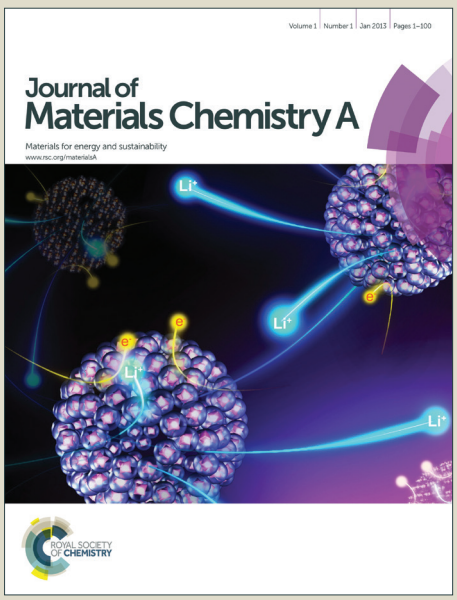

ROYAL SOCIETY OF CHEMISTRY

www.rsc.org/materialsA

Graphic abstract

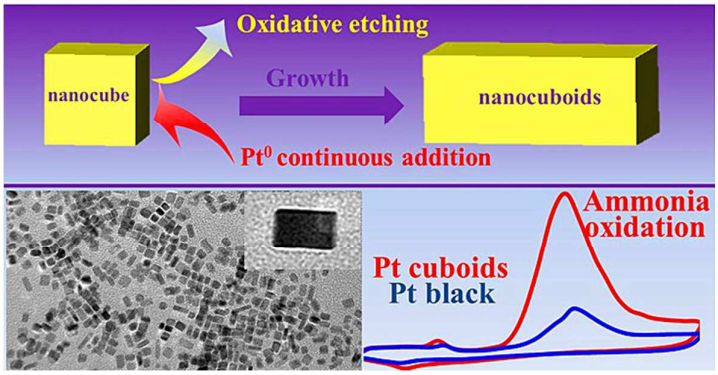

Pt-nanocuboids were synthesized by the simple hydrothermal method with the assistance of L-Lysine, exhibiting enhanced catalytic activity towards ammonia oxidation.

Journal of
Materials Chemistry A

RSCPublishing

ARTICLE

L-Lysine mediated synthesis of platinum nanocuboids and their electrocatalytic activity towards ammonia oxidation†

Geng-tao Fu,[a] Chang Liu,[a] Rui Wu,[a] Yu Chen,[a,b] Xiao-shu Zhu,*[a] Dong-mei Sun,[a] Ya-wen Tang,*[a] and Tian-hong Lu[a]

Cite this: DOI: 10.1039/x0xx00000x

Received 00th January 2012,
Accepted 00th January 2012

DOI: 10.1039/x0xx00000x

www.rsc.org/

Well-defined platinum nanocrystals with cuboid-like shape (Pt nanocuboids) were synthesized in high yields by the simple hydrothermal reduction of Pt(II) precursors with formaldehyde (HCHO) solution in the presence of L-lysine and polyvinyl pyrrolidone (PVP). The influential effects of several important experimental parameters on shape of Pt nanocrystals were systematically investigated, demonstrating that L-lysine and oxidative etching were critical to the morphological control and evolution of Pt nanocuboids. Due to the unique orientation and size effects, as-prepared Pt nanocuboids exhibited significantly enhanced catalytic activity and stability towards ammonia oxidation reaction (AOR) in comparison with commercial Pt black catalysts.

Introduction

During the past decades, the ammonia oxidation reaction (AOR) has attracted a great deal of attention due to their potential applications in wastewater treatment, hydrogen storage, and fuel cells (including direct ammonia fuel cells, solid oxide fuel cells).[1-6] Compared to various conventional fuel cells, such as methanol, ethanol, and formic acid fuel cells, the direct ammonia fuel cells in alkaline media have significant advantage in clean energy supply, such as no contamination and no carbon dioxide (CO_2) emission, because only nitrogen (N_2) and water (H_2O) are produced during reaction.[3, 6] In addition, ammonia is also easier to produce, store and transport than methanol, ethanol, and formic acid, which facilitates their commercialization.

The electrocatalytic activity of platinum (Pt) nanocrystals greatly depends on their morphology and surface crystalline orientation.[4-11] Consequently, increasing attentions have been paid to synthesize Pt nanocrystals with specific morphology and surface crystalline orientation in order to address the sluggish kinetic rate of the AOR.[4-9] For example, the Pt nanodendrites have been demonstrated as effective and highly active electrocatalysts for AOR due to the high accessibility of guest species, and the rich edges and corner atoms (*i.e.*, morphological effect).[4] In particular, the Vidal-Iglesias group demonstrated that the {100}-enclosed Pt nanocrystals exhibit much higher AOR activity than other low-index Pt nanocrystals including Pt {111} and {110} facets (i.e., orientation effect).[5] In comparison with commercial Pt/C, the AOR activity on carbon-supported cubic Pt nanocrystals (PtNC/C) enclosed by active {100} facets exhibits an enhanced activity and better durability.[6] Besides the morphology and surface crystalline orientation, the smaller size of the nanocrystals, which is associated with the higher surface to volume ratio, plays a more important role in the catalytic performance of the electrocatalysts. Therefore, the design and synthesis of Pt nanostructures with specific morphology, surface crystalline orientation and small size are critical for their application in AOR.

More recently, the specific adsorption of small molecules on the Pt-based nanocrystals surface has emerged as a promising strategy to control the surface structure.[12-17] For instance, the co-adsorption of carbon monoxide (CO) and amine makes Pt{100} more energetically stable than Pt{111}, which results in the formation of Pt nanocubes.[12] Glycine prefers to adsorb on Pt high-index {hk0} surface and facilitates the growth of Pt concave nanocubes, exhibiting extraordinary electrocatalytic activities towards the electrooxidation of methanol and formic acid.[16] The Pt-based nanocrystals with diverse shapes, such as cubes,[12, 13] concave cubes,[16] stars,[17] octahedral frames,[14] have been prepared with the assistance of small molecules. However, the electrochemical behavior of these novel Pt nanomaterials towards AOR has remained unclear, which requires further investigation.

Herein, we newly develop a simple and efficient strategy for the direct synthesis of cuboid-like Pt nanocrystals (named as Pt nanocuboids) with the assistance of basic amino acid molecules (L-Lysine). L-lysine (scheme 1), comprises two amine and one carboxyl groups, which provide both positive ($–NH_2^+$) and negative ($–COO^-$) ending groups. In reaction system, L-Lysine serves as a shape control agent, HCHO acts as a reductant, and PVP acts as a stabilizing agent and co-reductant. The resultant Pt

nanocuboids exhibit enhanced electrocatalytic activity and stability towards AOR compared to commercial Pt black catalyst, owing to the abundant exposed {100} facets and small particle size of Pt nanocuboids.

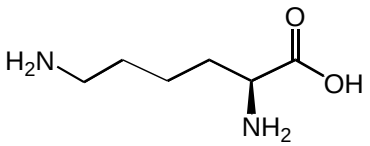

Scheme 1. Structure of L-Lysine molecule.

Experimental

Reagents and chemicals

L-Lysine was purchased from Shanghai kayon Biological Technology CO., Ltd. (Shanghai, China). Polyvinyl pyrrolidone (PVP, MW = 30000), Potassium tetrachloroplatinate(II) (K_2PtCl_4) and formaldehyde solution (HCHO, 40%) were purchased from Sinopharm Chemical Reagent Co. Ltd. (Shanghai, China). Commercial Pt black and Pt/C was purchased from Johnson Matthey Corporation. All reagents were of analytical reagent grade and used without further purification.

Preparation of the Pt nanocuboids

In a typical synthesis, 1.0 mL of 0.05 M K_2PtCl_4 solution, 0.5 mL of 0.5 M L-Lysine, and 50 mg PVP (MW = 30000) were added into 8.0 mL deionized water with continuous stirring for 10 minutes at room temperature. After adjusting the solution pH to 9.0, 1.0 ml of formaldehyde solution (HCHO, 40%) was rapidly added into the mixture solution. Then, the mixture was transferred to a 20 mL Teflon-lined stainless steel autoclave and heated at 160 °C for 4 h. After being cooled to room temperature, the obtained Pt nanocuboids were separated by centrifugation at 20 000 rpm for 15 min, washed several times with ethanol solution, and then dried at 60 °C for 5 h in a vacuum dryer.

Physical characterizations

Transmission electron microscopy (TEM) measurements were made on a JEOL JEM-2100F transmission electron microscopy operated at an accelerating voltage of 200 kV. The samples were prepared by placing a drop of the colloidal solution or catalyst powder dispersion in ethanol solution (99%) on a carbon film coated Cu grid (3 mm, 300 mesh), followed by drying under ambient conditions. Energy dispersive X-ray (EDX) analysis of particles was carried out on a JEOL JSM-7600F SEM. X-ray diffraction (XRD) patterns of nanocrystals were obtained with Model D/max-rC X-ray diffractometer using Cu Ka radiation source (λ=1.5406 Å) and operating at 40 kV and 100 mA. X-ray photoelectron spectroscopy (XPS) measurements were performed with a Thermo VG Scientific ESCALAB 250 spectrometer with a monochromatic Al Ka X-ray source (1486.6 eV photons), and the vacuum in the analysis chamber was maintained at about 10^{-9} mbar. The binding energy was calibrated by means of the C1s peak energy of 284.6 eV. The ultraviolet and visible spectroscopy (UV–vis) datas were recorded at room temperature on a Cary 50 spectrophotometer equipped with 1.0 cm quartz cells. Fourier transform infrared (FT-IR) measurements were carried out a Bruker tensor 27 FT-IR spectrometer.

Electrochemical measurements

All electrochemical experiments were performed using a CHI 660 C electrochemical analyzer (CH Instruments, Shanghai, Chenghua Co.). A standard three electrode system was used for all electrochemical experiments, which consisted of a Pt wire as the auxiliary electrode, a saturated calomel reference electrode (SCE), and a catalyst modified glassy carbon electrode as the working electrode. All potentials in this study were reported with respect to the SCE. All electrochemical measurements were carried out at 30 °C.

Before the preparation of catalyst ink, the Pt nanocuboids were irradiated with the UV irradiation (185 and 254 nm) in air for 4 h to remove the capping agents (i.e., PVP and L-Lysine).[15, 16, 18-21] An evenly distributed suspension of catalyst was prepared by ultrasonic the mixture of 10 mg catalyst and 5 mL H_2O for 30 min, and 6 μL of the resulting suspension was drop-cast onto the surface of the glassy carbon electrode (3 mm diameter). After drying at room temperature, 3 μL of Nafion solution (5 wt. %) was covered on the modified electrode surface and allowed drying again. Thus, the working electrode was obtained, and the specific loading of metal on the electrode surface was about 170 μg cm^{-2}. Prior to electrochemical test, the catalyst coated electrodes were pretreated by cycling the potential between −0.2 and 1.2 V vs. SCE for 50 cycles to remove possible contaminants on Pt. Cyclic voltammetry (CV) measurements were conducted in N_2-saturated 0.5 M H_2SO_4 aqueous solution. The ammonia oxidation reaction (AOR) experiments were conducted in N_2-saturated 1.0 M KOH solution with 0.1 M NH_4OH.

Results and discussion

Characterization of the Pt nanocuboids

The morphology of the Pt nanocrystals was investigated by TEM. As observed in Fig. 1A-B, the as-prepared Pt nanocrystals are well-defined and preserve a cuboid-like shape (90.0% cuboids, 8.0% cubes, and 2% irregular shapes) with aspect ratios of 1-3. According to particle size distribution histogram of as-prepared Pt nanocuboids, the average length and width of Pt nanocuboids are estimated to be ca. 5.8 nm and ca. 3.0 nm, respectively (Fig. 1C). The high resolution TEM (HRTEM) image (Fig. 1D) and the profile of the lattice fingers of the Pt nanocuboids (Fig. 1E) show the lattice fringes with an inter-fringe distance of 0.200, close to the lattice spacing of the {100} facets in the face centered cubic *(fcc)* Pt crystal (0.196 nm). The corresponding selected-area electron diffraction (SAED) pattern of the individual Pt nanocuboids shown in Fig. 1D (red square) indicates that Pt nanocuboids have single-crystalline nature with {100} lattice facet as the basal surfaces (Fig. 1F). According to the ideal structure model of Pt nanocuboids (insert in Fig. 1B), we

presumed each nanocuboid consists of six {100} facets. After titling sample 15 °C, a perpendicular edge (see white line) still is observed, confirming as-prepared Pt nanocrystals are four fold symmetric nanocuboids rather than nanorods (Fig. 1G).

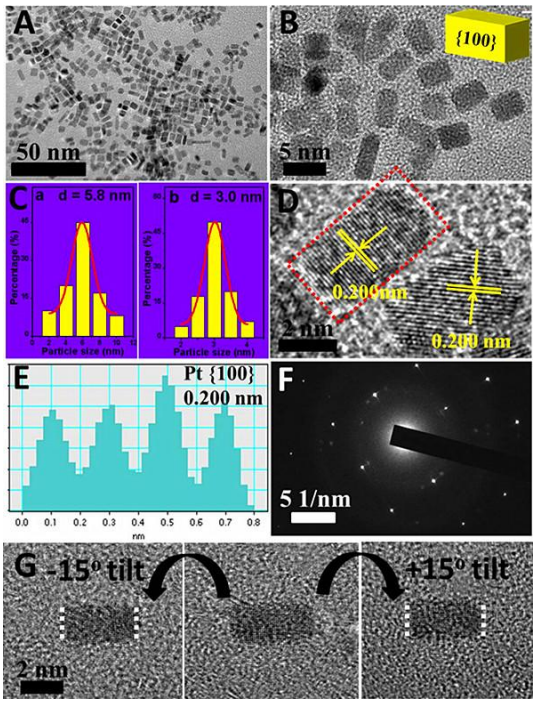

Fig. 1 (A) Typical TEM and (B) magnified TEM images of Pt nanocuboids, top-right inset in Figure 1B show the ideal structure model of the nanocuboids. (C) The corresponding size distribution histogram of Pt nanocuboids shown at Figure 1A: (a) length dimension, (b) width dimension. (D) HRTEM image of Pt nanocuboids. (E) The profile of the lattice fringes of Pt nanocuboids with {100} facets in Figure D. (F) The SAED pattern of Pt nanocuboids taken from region marked by red square in Figure D. (G) TEM images of an individual Pt nanocuboid at different angles.

The crystal structure and chemical composition of the as-synthesized Pt nanocuboids were characterized by EDX and XRD. EDX analysis demonstrates that Pt nanocuboids mainly contain Pt element (Fig. 1S). XRD pattern shows Pt nanocuboids have four peaks corresponding to the (111), (200), (220) and (311) facets of *fcc* Pt (JCPDS no. 04-0802), respectively (Fig. 2A). Meanwhile, the intensity ratio of (111) peak to (200) peak for Pt nanocuboids is about 1.74, which is much smaller than those of the commercial Pt black (2.28, Fig. S2) and standard Pt JCPDS data (2.16), confirming that the nanocuboids have a {100} dominated crystalline structure.[22,23] According to the Scherrer equation,[24-26] the average particle sizes of Pt nanocuboids and commercial Pt black are calculated to be 3.3 nm and 8.5 nm, respectively. XPS measurement demonstrates that the binding energy of $Pt4f_{5/2}$ and $Pt4f_{7/2}$ at 74.66 and 71.72 eV (Fig. 2B), respectively, referring to C1s=284.6 eV, and the interval was 3.39 eV, which are almost coincident with the standard values of bulk Pt (74.25 and 70.90 eV). By measuring the relative peak areas, it is found that the percentage of Pt^0 species in Pt nanocuboids is 87.9%, indicating that Pt^{II} precursor is successfully reduced to form metallic Pt in our synthesis.

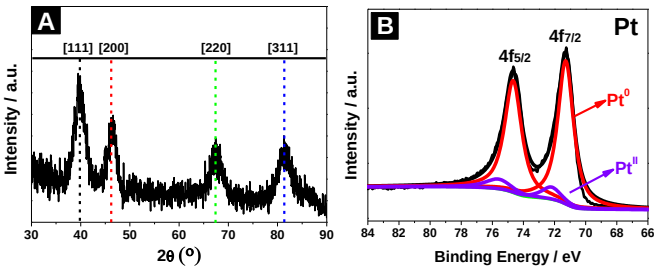

Fig. 2 (A) XRD pattern of Pt nanocuboids. (B) XPS spectrum of Pt nanocuboids in the Pt 4f region.

Formation mechanism of the Pt nanocuboids

In order to probe the possible growth mechanism of Pt nanocuboids, a series of controlled experiments were conducted. The effect of PVP on the morphology of the product was first investigated. In the absence of PVP, the obtained products consist mainly of irregular nanoparticles with obvious aggregation (Fig. 3A), indicating PVP acts as a stabilizing agent preventing the aggregation of the Pt nanoparticles. Notably, under the same conditions, Pt(II) ions also can be reduced by PVP in absence of HCHO (Fig. 3B), demonstrating PVP not only acts as stabilizing agent but also acts as a co-reductant. HRTEM image clearly shows the lattice fringes with an inter-fringe distance of 0.230 nm (insert in Fig. 3B), similar to Pt {111} facets in *fcc* Pt crystal (0.226 nm), indicating PVP doesn't make important contributions to the formation of Pt {100} facets under the present expermential conditions. When acetaldehyde (CH_3CHO) was used instead of HCHO, the cuboid-like Pt nanocrystals also can be obtained (Fig. S3), suggesting the aldehyde group (—CHO) is critical to formation of cuboid-like nanostructure. More importantly, it is worth noting that the use of L-Lysine is also critical to control the morphologies of Pt nanocrystals and the reduction kinetics. As observed in Fig. 3C, no cuboid-like nanocrystals are obtained without the addition of L-Lysine, but mixed morphologies including spheric-like nanocrystals and other irregular nanocrystals.

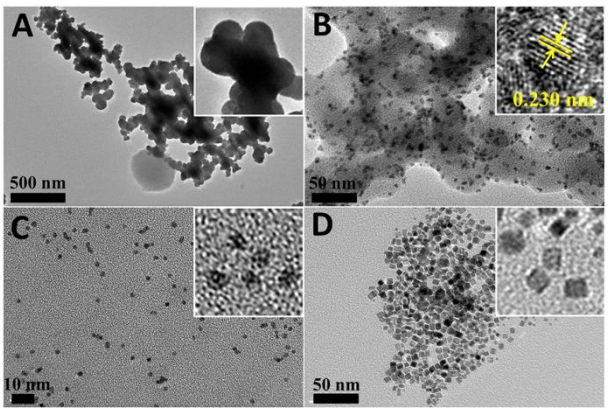

Fig. 3 TEM images of the product prepared using the standard procedure except for the exclusion of (A) PVP, (B) HCHO and (C) L-Lysine. (D) TEM image of Pt nanocrystals prepared by displacing the air with N_2 to eliminate typical etchant O_2. The top-right insets in Figure 3A-D show the corresponding magnified Pt nanoparticles.

Previous reports have documented that the metal cations could coordinate with amino acid molecule,[14-16, 27] which was confirmed by UV–vis measurement (Fig. S4). Obviously, UV–vis spectra of K_2PtCl_4 change after adding L-Lysine solution, confirming that L-Lysine has a coordination ability for K_2PtCl_4. The coordination interaction between K_2PtCl_4 and L-Lysine was further explored by linear sweeping voltammetry (Fig. S5). After adding L-Lysine into K_2PtCl_4 solution, the reduction peak potential of Pt^{II} species remarkably negatively shifts (-0.656 V vs. -0.353 V (vs. SCE)), indicating that the L-Lysine can decrease the reduction rate of Pt^{II} species due to the formation of the L-Lysine-Pt^{II} complex. Obviously, The particular coordination interaction between K_2PtCl_4 and L-Lysine is favorable for the morphological growth of Pt nanocuboids due to lower reduction potentials and slower reduction rate. Additionally, the FT-IR spectrum of Pt nanocuboids is similar to that of pure L-Lysine (Fig. S6), indicating that L-Lysine can intensively bind on Pt nanocuboids surface. According to the results, we presume that the critical role of L-Lysine in the formation of cuboid-like nanostructures might originate from the selective binding of L-Lysine on Pt nanocuboids surface during growth, which control the reduction and growth kinetics to generate well-defined nanostructures.

In particular, the like-cube Pt nanocrystals are obtained under N_2-saturated experimental conditions (Fig. 3D), suggesting O_2 is essential for the formation of Pt nanocuboids. Herein, we assume that well-defined cuboid-like Pt nanocrystals can be generated from cube by an appropriate degree of oxidative etching. Detailedly speaking (Fig. 4), the oxidative etching makes one {100} facet become more active than others and thus provides favorable sites for the addition of Pt atoms. When sufficient Pt atoms are added to the etched sites, atomic addition will be faster than the dissolution of atoms caused by etching. We believe that it is preferential growth at these active sites that led to the formation of nanocuboids, the six faces of which are bound by {100} facets. Conversely, spheric Pt nanocrystals are obtained when the oxidative etching is greatly enhanced by displacing the air with O_2 (Fig. S7). Likely, redundantly etching is active on the entire nanoparticle surface rather than locally on a specific face,[28] resulting in the formation of spheric Pt nanocrystals. The results demonstrated that localized oxidative etching is critical to the formation of Pt nanocuboids.

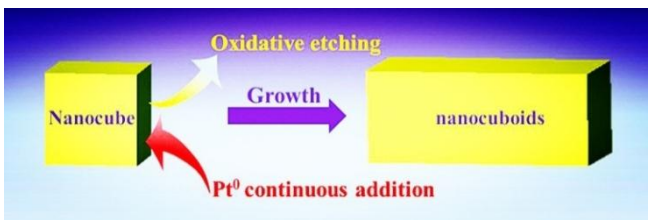

Fig. 4 The schematic illustration of the mechanisms responsible for the formation of Pt nanocuboids.

Usually, the formation of well-defined noble metal nanostructures is highly dependent on the precursor concentrations and reaction temperatures. As shown in Fig. S8, appropriate Pt^{II} precursor concentration facile the formation of well-defined Pt nanocuboids (Fig. S8B). In contrast, the lower Pt^{II} precursor concentration results in incomplete morphology (Fig. S8A) and the higher concentration doesn't not help to form uniform cuboid-like Pt nanostructures (Fig. S8C-D). Likely, the higher Pt^{II} concentration enhances the reaction rate greatly, thereby leading to changes in the morphology of Pt nanocuboids. The size of Pt nanocuboids can be conveniently controlled by increasing the reaction temperatures (Fig. S9), suggesting that the faster growth rate at higher temperature leads to the formation of larger-sized Pt nanocrystals. These experiments indicate that, by controlling the Pt^{II} precursor concentrations and reaction temperatures, cuboid-like Pt nanocrystals with well-defined morphology and controlled size can be realized.

Electrochemical test

The ammonia oxidation reaction (AOR) is highly structure sensitive reaction, which takes place much more active on Pt {100} facets than Pt {111} facets.[5, 6, 8, 9] Therefore, AOR was studied as a model reaction to probe the facet-dependent catalytic activity of {100}-enclosed Pt nanocuboids, and the result was compared with that of commercial Pt black enclosed by abundant {111} facets. Before the preparation of catalyst ink, the Pt nanocuboids were irradiated with the UV irradiation (185 and 254 nm) in air for 4 h to remove the capping agents (i.e., PVP and L-Lysine).[15, 16, 18-21] After UV/Ozone cleaning, the N 1s peak can not observed clearly, indicating that the capping agents on Pt nanocuboids surface have been effectively removed (Fig. S10). The electrochemical properties of Pt nanocuboids and commercial Pt black were investigated by CV in N_2-saturated 0.5 M H_2SO_4 solution (Fig. 5A). The electrochemically active surface area (ECSA) of catalysts was calculated by measuring hydrogen adsorption charge.[29, 30] The ECSA of nanocuboids (19.1 $m^2\ g^{-1}$) is slightly larger than that of the Pt black (17.6 $m^2\ g^{-1}$), attributing to smaller particle size of the nanocuboids (width: ca. 3.0 nm; length: ca. 5.8 nm) than that of Pt black (ca. 8.5 nm). Unlike the commercial Pt black, the CV of Pt nanocuboids shows a relatively intense peaks at 0 V and 0.1 V (vs. SCE) due to the characteristic H-adsorption features at the Pt {100} facets and {100} terraces,[6, 9] which provide further evidence that the prepared nanocuboids are primarily enclosed by Pt {100} facets.

The mass activity (the currents are normalized with reference to Pt mass) of the two different catalysts were invstigated in a mixture of 1 M KOH + 0.1 M NH_4OH solution (Fig. 5B). Obvious, Pt nanocuboids exhibits a current of 300.0 mA mg^{-1} at oxidation peak potential, which is ca. 3.7 times higher than that on Pt black (81.3 mA mg^{-1}). Meanwhile, onset oxidation potential of AOR on Pt nanocuboids negatively shift ca. 25 mV compared to Pt black, exhibiting an enhancement towards AOR in the low potential region. The higher ammonia oxidation current and the lower onset potential indicate that Pt nanocuboids have much better electrocatalytic activity. It is worth noting that the peak current of AOR on Pt nanocuboids is also much higher than those on the previously reported commercial Pt/C (ca. 50 mA mg^{-1}) and nanosheets (ca. 75 mA mg^{-1}) under the same reaction conditions,[31]

indicating that Pt nanocuboids are highly active for the AOR. In addition, it is observed that the mass activity of the 20 wt.% Pt nanocuboids/XC-72 is also higher than that of 20 wt.% commercial Pt/C at oxidation peak potential (Fig. S11), further indicating Pt nanocuboids hold promise as potentially practical electrocatalysts for the AOR. The specific activities of Pt nanocuboids and commercial Pt black for AOR were also investigated by CV (the current densities were normalized with reference to ECSA values of catalysts). The oxidation peak current density on Pt nanocuboids is 2.69 times higher than that on the Pt black (Fig. 5C).

The reaction mechanism of AOR on Pt undergo the dehydrogenation step ($NH_{3,ads} \rightarrow NH_{x,ad}$ (x=1, 2)) and rate limiting step ($NH_{x,ad} \rightarrow N_2H_{y,ad}$ (y=2–4)), then further dehydrogenation of the reaction intermediates leads to the final product (N_2).[32] Among the intermediates, N_{ad}, is considered a poisoning species which can strongly absorb to Pt surface and largely suppress AOR activity due to blocking the active sites. Notably, the N_{ad} species is produced more slowly and less stabilized on Pt {100} facets than those on Pt {111} and {110} facets.[6, 8, 33] Thus, the pronounced electrocatalytic activity of Pt nanocuboids can be attributed to their special surface crystalline orientation with abundant exposed [34] facets (i.e., orientation effect). In order to confirm this mechanism, the electrocatalytic activity of the ca. 5 nm Pt nanocubes with{100} facets towards the AOR was also conducted. As observed, the oxidation peak current density on Pt nanocubes is much higher than that on the Pt black, and close to the Pt nanocuboids (Fig. S12), indicating Pt {111} facets on Pt nanocuboids contribute to ehanced electrocatalytic activity. Meanwhile, the smaller particle size of Pt nanocuboids (3.3 nm) than that of Pt black (8.5 nm) increases the surface to volume ratio, which is also responsible for the improved electrocatalytic activity (i.e., size effect).

Additionally, the long term catalytic stability towards AOR was confirmed by chronoamperometric experiments at -0.3V for 6000 s (Fig. 5D). Compared to commercial Pt black, Pt nanocuboids exhibit a slower current attenuation with much high retention of current during the entire time range, revealing that Pt nanocuboids effectively promote catalytic stability as well as activity for the FOR. The improved stability of Pt nanocuboids most likely originate from the less N_{ad} species binding on Pt {100} facets,[6] due to N_{ad} species have lower adsorption energy on Pt {100} facets than on Pt {111}.

Conclusions

In summary, we successfully synthesized Pt nanocuboids enclosed {100} facets via a facile one-pot hydrothermal route with the assistance of L-Lysine molecules. The systematic studies demonstrated that L-Lysin and oxidative etching were critical to the formation of nanocuboids enclosed by {100} facets during the synthesis process. In addition, Pt nanocuboids showed the enhanced electrocatalytic activity and durability towards AOR relative to commercial Pt black due to a combination of orientation and size effects. The key finding demonstrated that L-Lysine mediated synthesis of Pt nanocuboids could be regarded as an effective and potential way to enhance the electrocatalytic activity of nanoparticles towards AOR.

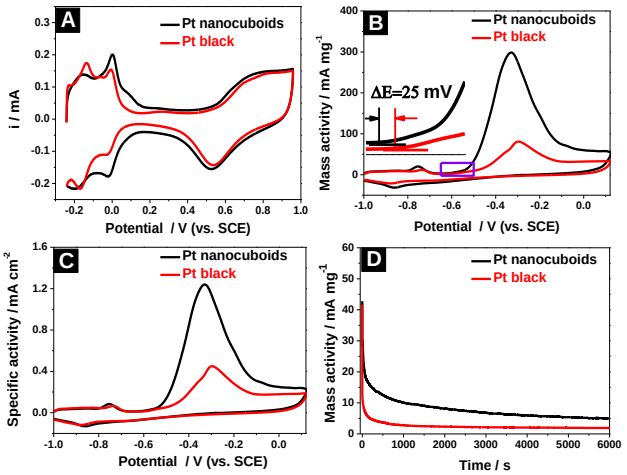

Fig. 5 (A) Pt nanocuboids and commercial Pt black in N_2-saturated 0.5 M H_2SO_4 solution at the scan rate of 50 mV s^{-1}. (B) The Pt mass-normalized and (C) ESCA-normalized cyclic voltammograms for Pt nanocuboids and commercial Pt black in N_2-saturated 1 M KOH + 0.1 M NH_4OH solution at the scan rate of 10 mV s^{-1}. (D) Chronoamperometry curves for Pt nanocuboids and commercial Pt black in N_2-saturated 1 M KOH + 0.1 M NH_4OH solution for 6000 s at -0.30 V potential.

Acknowledgments

The authors are grateful for the financial support of NSFC (21473111, 21376122 and 21273116), Natural Science Foundation of Jiangsu Province (BK20131395), United Fund of NSFC and Yunnan Province (U1137602), Industry-Academia Cooperation Innovation Fund Project of Jiangsu Province (BY2012001), and a project funded by the Priority Academic Program Development of Jiangsu Higher Education Institutions.

Notes and references

[a] *Jiangsu Key Laboratory of New Power Batteries, Jiangsu Collaborative Innovation Center of Biomedical Functional Materials, Analysis and Testing Center, School of Chemistry and Materials Science, Nanjing Normal University, Nanjing 210023, China*
[b] *School of Materials Science and Engineering, Shaanxi Normal University, Xi'an 710062, China*
Fax: +86–25–83243286; Tel: +86–25–85891651;
E–mail: xiaoshu_zhu78@163.com (X. S. Zhu)
tangyawen@njnu.edu.cn (Y. W. Tang)

† Electronic Supplementary Information (ESI) available: Additional characterization data. See DOI: 10.1039/b000000x/

1 L. Cunci, C. A. Velez, I. Perez, A. Suleiman, E. Larios, M. Jos é-Yacam án, J. J. Watkins and C. R. Cabrera, *ACS Appl. Mater. Interfaces*, 2014, 6, 2137-2145.
2 H. Kim, D. Won, K. S. Nahm and P. Kim, *Catal. Lett.*, 2014, 144, 469-477.
3 C. Zhong, W. Hu and Y. Cheng, *J. Mater. Chem. A*, 2013, 1, 3216-3238.
4 J. Liu, W. Hu, C. Zhong and Y. F. Cheng, *J. power sources*, 2013, 223, 165-174.

5 F. J. Vidal-Iglesias, J. Solla-Gullón, V. Montiel, J. M. Feliu and A. Aldaz, *J. Phys. Chem. B*, 2005, 109, 12914-12919.
6 C. Zhang, S. Y. Hwang and Z. Peng, *J. Mater. Chem. A*, 2013, 1, 14402-14408.
7 J. Liu, C. Zhong, Y. Yang, Y. Wu, A. Jiang, Y. Deng, Z. Zhang and W. Hu, *Int. J. Hydrogen Energy*, 2012, 37, 8981-8987.
8 F. Vidal-Iglesias, N. García-Aráez, V. Montiel, J. Feliu and A. Aldaz, *Electrochem. Commun.*, 2003, 5, 22-26.
9 R. A. Martínez-Rodríguez, F. J. Vidal-Iglesias, J. Solla-Gullón, C. R. Cabrera and J. M. Feliu, *J. Am. Chem. Soc.*, 2014, 136, 1280-1283.
10 B. Y. Xia, H. B. Wu, Y. Yan, X. W. Lou and X. Wang, *J. Am. Chem. Soc.*, 2013, 135, 9480-9485.
11 B. Y. Xia, W. T. Ng, H. B. Wu, X. Wang and X. W. D. Lou, *Angew. Chem. Int. Edit.*, 2012, 124, 7325-7328.
12 B. H. Wu, N. F. Zheng and G. Fu, *Chem. Commun.*, 2011, 47, 1039-1041.
13 Y. Kang, X. Ye and C. B. Murray, *Angew. Chem. Int. Edit.*, 2010, 49, 6156-6159.
14 X. Wang, F. Nosheen, Z. C. Zhang and J. Zhuang, *Nanoscale*, 2013, 5, 3660-3663.
15. Z. Zhang, Y. Yang, F. Nosheen, P. Wang, J. Zhang, J. Zhuang and X. Wang, *Small*, 2013, 9, 3063-3069.
16 Z. C. Zhang, J. F. Hui, Z. C. Liu, X. Zhang, J. Zhuang and X. Wang, *Langmuir*, 2012, 28, 14845-14848.
17 X. Huang, Z. Zhao, J. Fan, Y. Tan and N. Zheng, *J. Am. Chem. Soc.*, 2011, 133, 4718-4721.
18 C. Wang, H. Daimon, Y. Lee, J. Kim and S. Sun, *J Am Chem Soc*, 2007, 129, 6974-6975.
19 M. Crespo-Quesada, J. M. Andanson, A. Yarulin, B. Lim, Y. Xia and L. Kiwi-Minsker, *Langmuir*, 2011, 27 7909–7916.
20 C. Aliaga, J. Y. Park, Y. Yamada, H. S. Lee, C.-K. Tsung, P. Yang and G. A. Somorjai, *J. Phys. Chem. C*, 2009, 113, 6150-6155.
21 Z. C. Zhang, J. F. Hui, Z. G. Guo, Q. Y. Yu, B. Xu, X. Zhang, Z. C. Liu, C. M. Xu, J. S. Gao and X. Wang, *Nanoscale*, 2012, 4, 2633-2639.
22 G. Fu, X. Jiang, M. Gong, Y. Chen, Y. Tang, J. Lin and T. Lu, *Nanoscale*, 2014, 6, 8226-8234.
23 R. Loukrakpam, P. Chang, J. Luo, B. Fang, D. Mott, I. T. Bae, H. R. Naslund, M. H. Engelhard and C. J. Zhong, *Chem. Commun.*, 2010, 46, 7184-7186.
24 X. Qiu, G. Fu, Y. Chen, Y. Tang and T. Lu, *J. Mater. Chem. A*, 2013, 1, 14874–14878.
25 J. Xu, G. Fu, Y. Tang, Y. Zhou, Y. Chen and T. Lu, *J. Mater. Chem.*, 2012, 22, 13585-13590.
26 F. Lan, D. Wang, S. Lu, J. Zhang, D. Liang, S. Peng, Y. Liu and Y. Xiang, *J. Mater. Chem. A*, 2013, 1, 1548-1552.
27 A. Iakovidis and N. Hadjiliadis, *Coordin. chem. rev.*, 1994, 135, 17-63.
28 Y. Xiong, H. Cai, B. J. Wiley, J. Wang, M. J. Kim and Y. Xia, *J. Am. Chem. Soc.*, 2007, 129, 3665-3675.
29 G. Fu, K. Wu, X. Jiang, L. Tao, Y. Chen, J. Lin, Y. Zhou, S. Wei, Y. Tang, T. Lu and X. Xia, *Phys. Chem. Chem. Phys.*, 2013, 15, 3793-3802.
30 G. Fu, R. Zhao, L. Ding, L. Tao, J. Lin, Y. Chen, Y. Tang, Y. Zhou and T. Lu, *ChemPlusChem*, 2013, 78, 623 – 627.
31 X. Du, Y. Yang, J. Liu, B. Liu, J. Liu, C. Zhong and W. Hu, *Electrochim. Acta*, 2013, 111, 562-566.
32 H. Gerischer and A. Mauerer, *J. Electroanal. Chem. Interfacial Electrochem.*, 1970, 25, 421-433.
33 V. Rosca and M. T. Koper, *Phys. Chem. Chem. Phys.*, 2006, 8, 2513-2524.
34 J. H. Yang, W. J. Zhou, C. H. Cheng, J. Y. Lee and Z. L. Liu, *ACS Appl. Mater. Interfaces*, 2010, 2, 119-126.

